
Article:
Ababei, Razvan V., Evans, Richard F.L., Agop, Maricel et al. (2024) Fractal perspective of RKKY exchange interactions in L10 FePt. Physical Review B. 094437. ISSN: 2469-9969

https://doi.org/10.1103/PhysRevB.109.094437

Fractal perspective of RKKY exchange interactions in $L1_0$ FePt

Razvan-V. Ababei [1,2] Richard F. L. Evans,[1] Maricel Agop,[3,4] and Roy W. Chantrell[1]

[1]*School of Physics, Engineering and Technology, University of York, York YO10 5DD, United Kingdom*

[2]*Research Center with Integrated Techniques for Atmospheric Aerosol Investigation in Romania, RECENT Air, Laboratory of Astronomy and Astrophysics, Astronomy Observatory, Alexandru Ioan Cuza University, 5-7 Mihail Sadoveanu, 700490 Iasi, Romania*

[3]*Department of Physics, Gheorghe Asachi Technical University of Iasi, 700050 Iasi, Romania*

[4]*Romanian Scientists Academy, 010071 Bucharest, Romania*

(Received 22 November 2023; accepted 11 March 2024; published 27 March 2024)

This paper introduces an approach to approximating exchange interactions in FePt, characterizing their effect on the Curie temperature and magnetic anisotropy, properties crucial for heat-assisted magnetic recording. The proposed model employs the Ruderman-Kittel-Kasuya-Yosida (RKKY) function, offering a different perspective on magnetization processes within finite FePt grains. The RKKY function is derived as a specific instance of a fractal curve, such as the Jacobi elliptical function. The study showcases a holographic implementation of these exchange interactions, translatable into an atomistic spin dynamics model, yielding valid outcomes for finite-size scaling laws. The primary goal is to formulate an approximate spin Hamiltonian with fewer neighbors, enhancing the efficiency of simulations for the FePt which is a candidate for heat-assisted magnetic recording media. Additionally, the research delves into how the number of interactions per bond impacts magnetization evolution across different temperatures and system sizes. Our findings suggest that this model is more computationally efficient for Monte Carlo simulations than the comprehensive density-functional-theory-based spin Hamiltonian proposed by Mryasov *et al.*

DOI: 10.1103/PhysRevB.109.094437

I. INTRODUCTION

$L1_0$ FePt exhibits suitable properties for recording media [1–3], particularly for heat-assisted magnetic recording (HAMR) [4,5]. Therefore, significant interest has been dedicated to understanding the exchange interaction, especially at lower dimensions of the particles where the FePt grains can lose their ferromagnetic properties. Any magnetic material can be described and identified with a mathematical object as fractal or multifractal when we try to describe its complex functionality and structural properties. In this sense, there are a few arguments that support this fractal/multifractal behavior:

(1) The given Eq. (1) incorporating a noninteger classical exponent with $\beta = 0.37$ is a specific example derived from the Curie-Bloch equation [6]. This equation describes the temperature-magnetization dependence and is further expanded by a more comprehensive equation proposed by Kuz'min *et al.* [7]:

$$m(\tau) = (1 - \tau^{\alpha})^{\beta}. \tag{1}$$

Here, $m = M_s/M_0$ represents the reduced saturation magnetization, α serves as a phenomenological exponent introduced to consider the quantum states of spins in proximity to the ground state, while τ represents the reduced temperature by Curie point as $\tau = T/T_C$, where T_C is the Curie temperature. In the Heisenberg approximation, α takes the integer value of 1, leading to a more simplified equation $m(\tau) = (1 - \tau)^{\beta}$.

(2) The phenomenological shift ν in the finite scale law which might vary between 0.65 and 0.73 as pointed out in Refs. [8,9].

(3) The existence of fractal structures such as magnetic fluxons [10], skyrmions [11,12], magnetic domains [13], and vortices [14]. In addition to this, fractal nucleation patterns were observed experimentally during the FePt/Fe reversal mechanism, as shown in Ref. [15], suggesting a different approach to exchange treatment using fractal/multifractal theory. We can classify, therefore, the magnetic structures depending on scale resolution by approaching a another perspective of scale relativity theory (SRT) [16,17] which might be suitable to describe the magnetization dynamics of magnetic materials, particularly the exchange energy of magnetic materials.

One reasonable approach is the first-principles exchange interactions presented in Refs. [18,19] where the exchange coupling constant follows an oscillatory dependence with the separation distance between atoms as shown in Fig. 1(c). We observed a similarity of this dependence with the Ruderman-Kittel-Kasuya-Yosida (RKKY) function [20–22] given by the following expression,

$$J(r) = J_0 \frac{\cos(r \cdot k_f)}{r^3}, \tag{2}$$

where k_f is the Fermi wave vector which depends on the lattice properties of the magnetic material such as lattice parameter, crystal order, and valence. Equation (2) might be an approximation of the elliptic function presented in the following section. For an fcc structure, the Fermi wave vector can be calculated as $k_f = (12\pi^2/a^3)^{1/3} \approx 4.90/a$ as shown in Ref. [23], where a is the lattice parameter. This rate of decay (r^{-3}) is suitable for this particular alloy. However, Rezaei *et al.* [24] demonstrated different exponential decay rates of r for

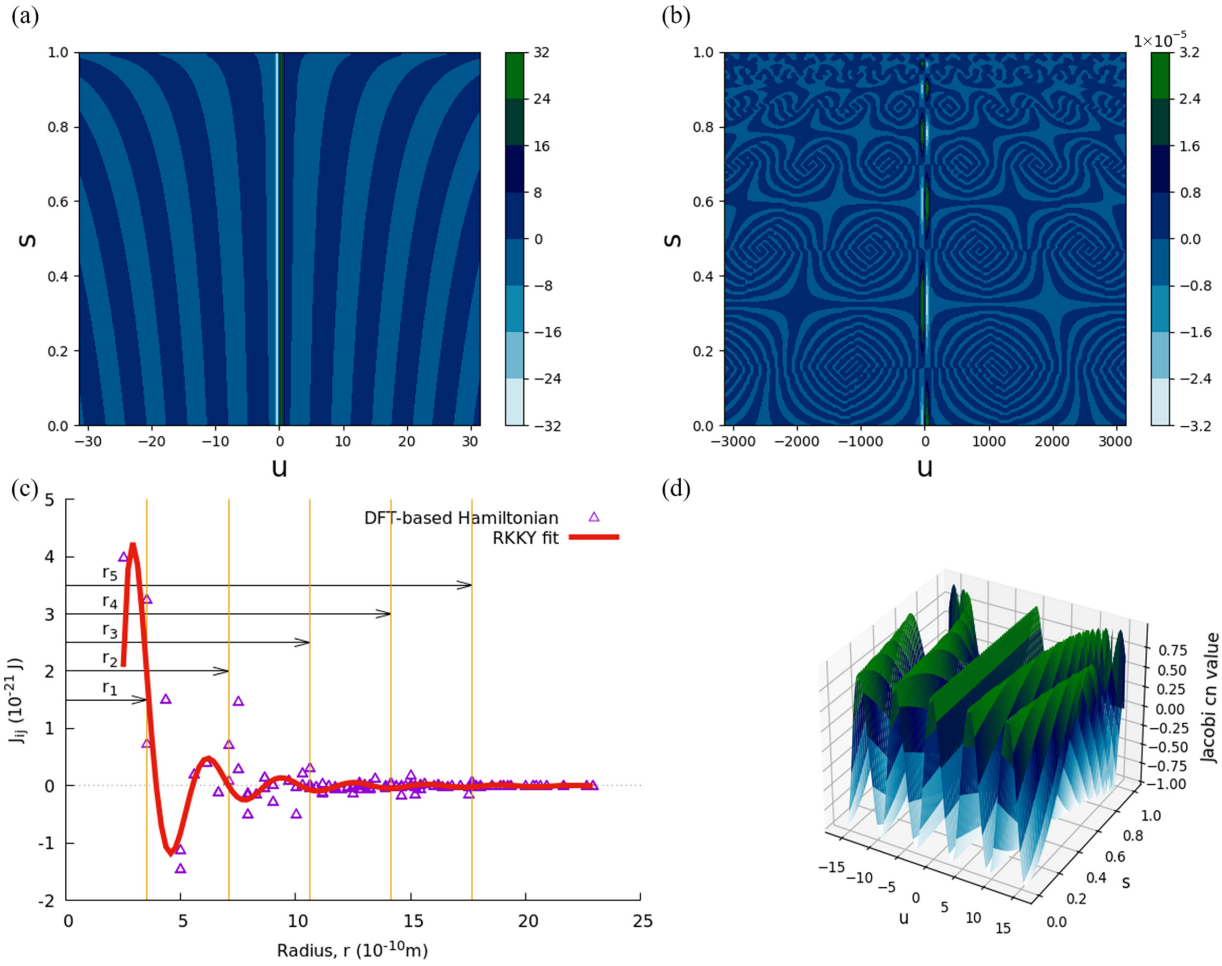

FIG. 1. Plot of Jacobi elliptic cn at different resolution scales: (a) and (b) show two-dimensional (2D) representations of $\frac{\mathrm{cn}(u\cdot k|s)}{u^3}$, where k is set at 0.98, s takes values from 0 to 1, and u has different scale resolutions. (c) shows the exchange constant values at different distances calculated within DFT. The solid line represents the fit using Eq. (2) giving a value for k_f around 0.98 nm^{-1}. (d) illustrates a 3D plot of $\mathrm{cn}(u, k)$ where u varies between -5π and 5π.

some alloys based on transition metals such as Fe, Mn, and Co. They found that n varies between 0.5 and 2 after fitting the calculated exchange interaction values within spin-polarized density functional theory (SP-DFT) using the following equation: $J(r) = J_0 \frac{\cos(2\cdot a\cdot k_f\cdot r)}{(2\cdot a\cdot k_f\cdot r)^n}$.

The RKKY function was initially developed to describe the nuclear magnetic moment [25] and then was expanded to describe the magnetic interaction in metals and nonmetals [24,26–28]. As shown in Fig. 1 the exchange values for different separations can be mapped onto the RKKY function, however, it is challenging to find the most accurate value for k_f to have the best depiction of the Mryasov *et al.* model [18]. Hence, in this study, we provide a comparison between the RKKY function derived from a fractal/multifractal function and the one obtained from a full-range Hamiltonian. This comparison aims to verify the validity of the exchange model.

II. THEORY AND COMPUTATIONAL METHODS

To describe the magnetic processes, especially magnetization dynamics, it is necessary to introduce the scale resolution both into the expression of the physical variables as well as into the expressions of the fundamental equation governing these magnetic nanomaterials. This mathematical method of describing the dynamics of complex magnetic nanomaterials implies the development of both new geometric structures and physical theories consistent with these geometric structures for which the laws of motion, invariant to time coordinate transformations, are also invariant to transformations with respect to scale resolution. Such a geometric structure is one based on the concept of the fractal/multifractal and the corresponding physical model described in the scale relativity theory (SRT) [16,29]. From this perspective, the holographic implementation in the description of the magnetization dynamics will be made explicit based on the continuous and nondifferentiable curves (fractal/multifractal curves).

We propose a function that might describe the strength of the exchange interaction in a variety of magnetic structures derived from the Jacobi cn elliptic function [30,31] shown in the equation

$$J(r) = J_0 \frac{\mathrm{cn}(k_j \cdot r|s)}{r^3}, \tag{3}$$

where the argument of the cn elliptic function, $k_j \cdot r$, is the phase associated with the separation between magnetic spins and s is the modulus of this function denoting the degree of

fractality. This complex function converges to the oscillating RKKY function shown in Eq. (2) depending on the fractality degree s. Hence, there are two boundary limits of the Jacobi cn elliptic function: (a) When $s \to 0$, then Eq. (3) becomes the same as Eq. (2), and (b) when $s \to 1$, then Eq. (3) becomes

$$J(r) = J_0 \frac{\mathrm{sech}(k \cdot r)}{r^3}. \tag{4}$$

Therefore, this RKKY function is a particular case of the cn elliptic function that might represent a more general description of the exchange interaction for complex magnetic materials such as $L1_0$ FePt. The oscillatory behavior can be observed in Fig. 1(a) where $\mathrm{cn}(u \cdot k|s)/u^3$ is plotted as a function of both parameters. Once the spatial resolution is enhanced by a factor, it becomes possible to detect fractal patterns illustrated in Fig. 1(b), resembling the formation of specific magnetic structures at the scale resolution of micromagnetics. The presence of doping and lattice defects is indicated by changes in the fractal dimension. A thorough investigation of this topic is an avenue for future research.

With this insight into the exchange interaction, we employed the atomistic spin model which is based on the Heisenberg Hamiltonian [32] given by the following equation:

$$\mathcal{H} = \mathcal{H}_{\mathrm{ex}} + \mathcal{H}_{\mathrm{ani}}. \tag{5}$$

Here, $\mathcal{H}_{\mathrm{ani}}$ represents the anisotropy term of the Hamiltonian which can be calculated as $\mathcal{H}_{\mathrm{ani}} = -k_u \sum_i (\mathbf{S}_z^i \cdot \mathbf{e})^2$, where k_u is the perpendicular anisotropy constant per atom and $\mathbf{e}$ denotes the direction of the anisotropy axis along the $\mathbf{z}$ direction. Here, we present two approaches to compute the exchange term for each atom. The first one is given by the list of long-range interactions based on DFT calculation presented in Refs. [18,19] where the exchange coupling constant is fully calculated for each atomic bond up to a radius of 5.5 unit cell (u.c.) size. The exchange coupling depends on the separation distance between the atoms, r_{ij}, where the nature of the exchange interaction can be ferromagnetic or antiferromagnetic as shown in Fig. 1(c). The number of interactions per atomic bond increases with the radius.

The second approach is the analytical expression following Eq. (2) for each atomic bond taking into account a specific number of neighbor interactions at different separations as shown in Fig. 1(c). The exchange term in this case can be expressed for a single atomic bond as

$$\begin{aligned}\mathcal{H}_{\mathrm{ex}}^i &= -\sum_j J_{ij}(r)\mathbf{S}_i \cdot \mathbf{S}_j \\ &= -\sum_j \begin{pmatrix} S_x^i & S_y^i & S_z^i \end{pmatrix} \begin{pmatrix} J_{xx} & 0 & 0 \\ 0 & J_{yy} & 0 \\ 0 & 0 & J_{zz} \end{pmatrix} \begin{pmatrix} S_x^j \\ S_y^j \\ S_z^j \end{pmatrix},\end{aligned} \tag{6}$$

where j is the number of interactions with the neighbors which depends on the range of the cutoff r as mentioned above. This corresponds to the coordination number for the nearest-neighbor approximation, r_1, where the list of interactions contains six interactions, the second range, r_2 involves 26 interactions, while r_3 involves 130, and r_5 involves a substantial 1978 interactions. $J_x(r_{ij}), J_y(r_{ij}), J_z(r_{ij})$ are the elements of the isotropic tensor $J_{ij}(r_{ij})$ which are calculated according to Eq. (2) as

$$\begin{aligned} J_x^{ij}(r_{ij}) &= J_x^0 \frac{\cos(k_f r)}{r_{ij}^3}, \\ J_y^{ij}(r_{ij}) &= J_y^0 \frac{\cos(k_f r)}{r_{ij}^3}, \\ J_z^{ij}(r_{ij}) &= J_z^0 \frac{\cos(k_f r)}{r_{ij}^3}. \end{aligned} \tag{7}$$

$J_{x,y,z}^0$ represents the exchange value constants with the nearest neighbors (NN) which can be extracted from Mryasov data by fitting them as shown in Fig. 1(c) and r_{ij} is the distance between two different atoms i and j. In the exchange list values of Mryasov *et al.* [19] a slight difference between the in-plane exchange value $J_{x,y}^0$ is noted compared with the out-of-plane component J_z^0. Here, $J_x^0 = J_y^0 < J_z^0$ where $(J_z^0 - J_{x,y}^0)/J_z^0 = 4.8\%$. This small difference generates an analogous two-ion contribution given by the Mryasov model, which is essentially an exchange anisotropy. This has a remarkable impact on the anisotropy rescaling shown later in this paper. Besides this, Hinzke *et al.* [19] demonstrated different domain wall widths in plane and perpendicular due to this special form of the Hamiltonian.

We modeled a cylindrical grain of $L1_0$ FePt with a lattice parameter of 3.54 Å, where the atoms are arranged in a simple cubic structure equivalent of measurements where the lattice parameter may vary depending on the experimental conditions shown in Ref. [33]. The magnetic moment has been set at $3.2\,\mu_B$ per atom which gives a saturation magnetization of 680.5 kA/m. We set a small uniaxial anisotropy of $k_u = 6.9 \times 10^{-23}$ J/atom. The simulations have been performed using the constrained Monte Carlo method described in Ref. [34] which is implemented in the VAMPIRE atomistic simulation software package [32]. It has gathered 100 000 Monte Carlo steps at every 10 K temperature step.

III. RESULTS

We have simulated a series of temperature-dependent magnetizations, calculating the distribution of Curie temperature at different sizes and truncation ranges of the neighbor exchange list. Here, we model a 10-nm-high FePt cylinder varying the basal diameter from 2 to 11 nm using both methods of parametrizing the exchange interaction list presented in the previous section.

Figure 2 shows a series of temperature magnetization curves for different diameters of the cylindrical grain at different cutoff ranges using the RKKY model of exchange values presented in the previous section by averaging 100 000 MC steps, in 10 K steps. In these simulations, we have not explored dimensions below 2 nm due to the experimental observations in Ref. [8], where it was demonstrated that the critical width for an $L1_0$ FePt grain is 3 nm. This specific size represents the minimum particle width that exhibits chemical ordering. Here, a significant drop in the magnetization is noticed for a specific range of cutoff, 3 unit cell size for example, and also for lower dimensions.

Figure 2 shows the temperature dependence of the magnetization for different ranges of the cutoff at different sizes

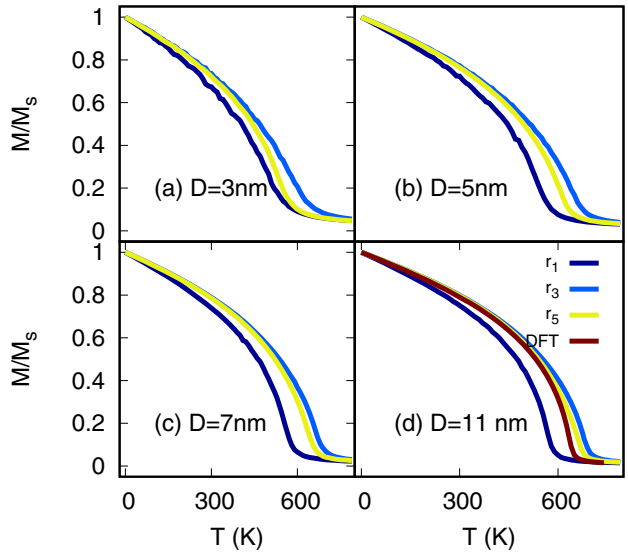

FIG. 2. The temperature magnetization dependence for different diameters of FePt cylinder and different cutoff ranges using the RKKY model of exchange interaction coupling.

of the diameter. For a higher-order range of cutoff, the decreasing rate of magnetization on temperature is similar for all diameters of particles higher than 3 nm. However, a notable discrepancy appears for the second range where the list of interactions incorporates a significant number of antiferromagnetic exchange types leading to a weak ferromagnetic phase of the simulated particle whereas the first order leads to a more rapid decrease of magnetization as it is approaching the Curie temperature.

In order to investigate the distribution of Curie temperature it has been extracted from each curve by fitting the dependence using the classical expression

$$m(T) = (1 - T/T_C)^{\beta}. \tag{8}$$

In Fig. 3, we present the Curie temperature's dependence on the system diameter across different ranges. Figure 3(a) illustrates the distribution of the Curie temperature using the list of DFT-based exchange interactions, while Fig. 3(b) showcases the same distribution utilizing the RKKY function. Notably, both models exhibit a consistent trend in Curie temperature distribution as a function of system size, aligning with prior calculations conducted by Hovorka *et al.* [9]. In order to explore the magnetic behavior at lower sizes, we fit each dependence of Curie temperature on diameter following the finite-size scaling law [35],

$$T_C(D) = T_C^{\text{bulk}}\left[1 - \left(\frac{d_0}{D}\right)^{-1/\nu}\right], \tag{9}$$

where ν is the phenomenological shift exponent and d_0 is the parameter related to unit cell size. For a better fitting, we calculated the T_C^{bulk} by simulating a particle with 15 nm diameter using periodic boundary conditions. This will give the bulk value for each case of the truncation range shown in Table I along with values for the shifting exponent which is extracted by applying Eq. (8) on the simulated distribution in Fig. 3.

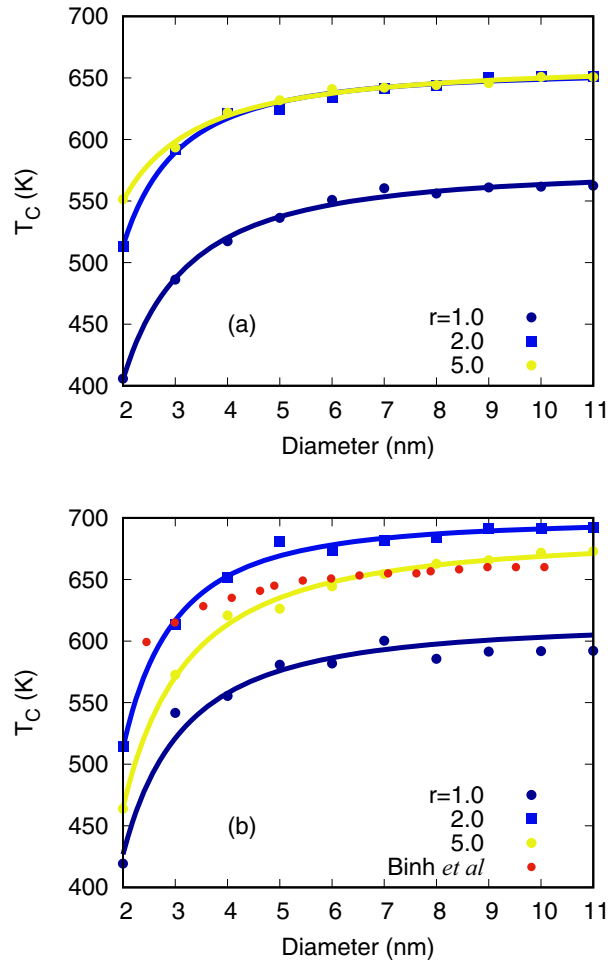

FIG. 3. The size distribution of Curie temperature for different ranges of cutoff. The solid lines stand for the fitting using Eq. (9). (a) shows the size distribution using the DFT-based Hamiltonian, and (b) corresponds to the RKKY model.

We noticed a rapid decrease in Curie temperature by approaching a diameter lower than 3 nm for both models at a higher range of cutoff (e.g., 5 u.c.). All these results are summarized in Table I, where T_C^{bulk} is close to the experimental value of 775 K [8] and the exponent ν which experimentally has been found around 0.91. The classical Heisenberg approach will give a value for the exponent at 0.71. However, the exponent ν and T_C^{bulk} decreases inconsistently with the list of the full range of exchange interactions for both cases which is essential in the understanding of the demagnetization processes at lower sizes where different truncations can

TABLE I. The bulk T_C and critical exponent ν for both models at different ranges of cutoff. The values have been obtained by fitting the graphs from Fig. 3 using Eq. (9).

Model	DFT-based			RKKY		
Range	r_1	r_2	r_5	r_1	r_2	r_5
T_C^{bulk}	576.27	655.84	661.70	594.55	698.29	682.04
ν	0.62	0.53	0.71	0.58	0.49	0.61

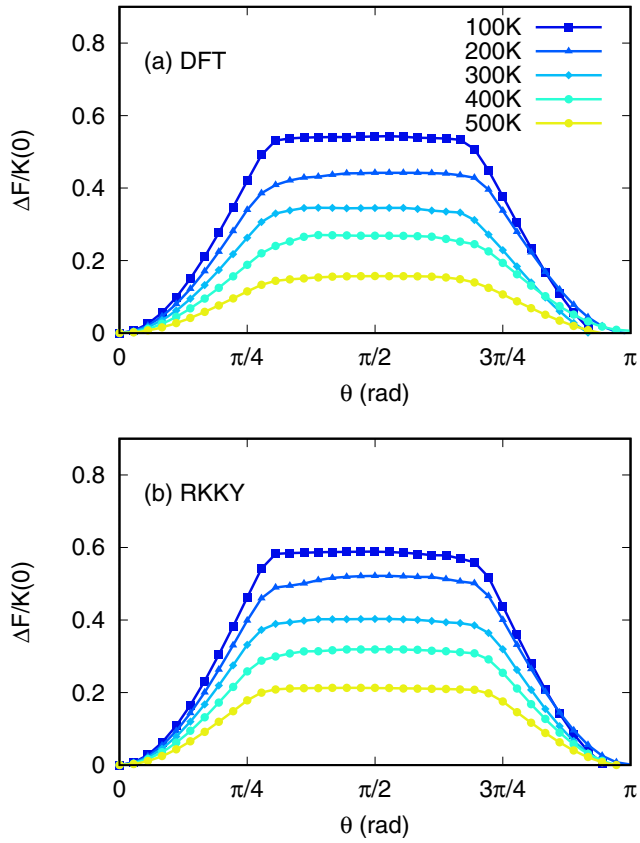

FIG. 4. Plot of reduced free energy $\mathcal{F}$ for a FePt cylinder with a basal diameter of 5 nm and a height of 10 nm using a full DFT-Hamiltonian and RKKY function up to 5 u.c. range at different simulation temperatures.

appear due to the sizes of the particle. For instance, a particle whose dimensions are below 3 nm cannot incorporate the full list of interactions for each atomic site. Hence, a random truncation can appear not only in computational models but also in the arrangement of atoms within a lower-size particle. In contrast to the findings of Binh *et al.* [36], as represented by the red data points in Fig. 3(b), our simulations differ significantly in terms of simulation details. Notably, we employ distinct material parameters, particularly concerning the lattice parameter and atomic moment. The presented method shows a more pronounced finite-size effect for a simple cubic structure.

The temperature-dependent anisotropy scaling has been investigated using constrained Monte Carlo (CMC) simulations by simulating the restoring torque from 0° to 180° with a step of 5°. By doing this we can find the free energy of the system by integrating the curve along the polar angle. This procedure is similar to the approach presented by Evans *et al.* in Ref. [37] where the free energy can be calculated through the following equation,

$$\mathcal{F} = \int_0^{\theta} \tau d\theta, \tag{10}$$

where τ is the restoring torque at a specific polar angle between magnetization and easy axis denoted by θ. The torque

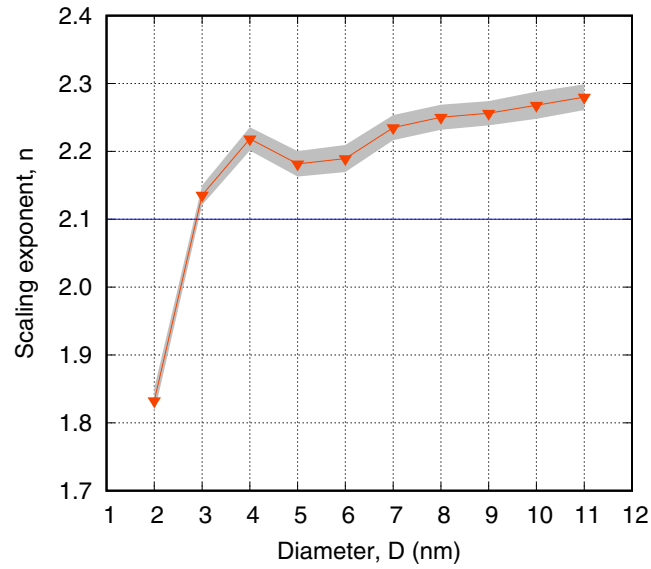

FIG. 5. Plot of scaling factor n as a function of diameter of the $L1_0$ FePt cylinder using the RKKY function with a two-ion contribution. The shaded gray area shows the minimum to the maximum range that the scaling factor might vary.

is computed for each individual spin as

$$\tau = -\sum_i \mathbf{S}_i \times \frac{\partial \mathcal{H}}{\partial \mathbf{S}_i}, \tag{11}$$

where $\mathcal{H}$ is the Hamiltonian according to Eq. (5) and $\mathbf{S}_i$ is the spin orientation.

A typical series of reduced free-energy curves is illustrated in Fig. 4 by performing a numerical integration of restoring torque along a polar angle, θ. Here, both the DFT-based Hamiltonian and RKKY model of exchange exhibit some deviation from the classical $\sin^2(\theta)$ dependence at increased polar angles due to the large two-ion anisotropy [19] term. Asselin *et al.* [34] demonstrated the impact of the two-ion term over the free energy giving different results from the classical form of torque as $\sin(\theta)^2$ being in agreement with our calculations presented here. With these results shown in Fig. 4(b), we can extract the anisotropy $K(T)$ at each simulation temperature by fitting the free-energy curves as a function of the polar angle θ for lower values of the angle below $\pi/4$ using the classical expression [37]

$$\mathcal{F} = K(T)\sin^2(\theta), \tag{12}$$

where $K(T)$ represents the anisotropy energy given by the anisotropic exchange mainly. The dependence of $\ln[K(T)/K(0)]$ as a function $\ln[M(T)/M(0)]$ obeys a linear function where the slope n is known as the scaling factor of anisotropy with reduced magnetization. Here, $K(0)$, $M(0)$ are the values of anisotropy energy and magnetization at 0 K.

Figure 5 shows the agreement of the scaling factor n of $\ln(K/K_0)$ vs $\ln(M/M_s)$ fitting with theoretical calculations [19,34], and experiment [38] is very close to 2.1 at a different radius of the cylindrical particles. This additional finite-size effect arises due to more correlated spins for smaller sizes, thus making the magnetic anisotropy larger than expected.

IV. CONCLUSIONS

To summarize, we have investigated two models of exchange interactions employing the atomistic spin model. Both models predict a reasonable temperature dependence which is necessary for developing new recording devices for heat-assisted magnetic recording (HAMR). Given the challenges linked to employing the complete Hamiltonian, an alternative approach involves integrating the RKKY model. This model can be regarded as a specific instance of the fractal model. By doing so, more insight into exchange interactions within atomistic and micromagnetic processes can be achieved. This entails establishing a connection between the lattice's disorder level and fractal dimensions. This aspect is currently under investigation in our ongoing research. Finally, the magnetic behavior at lower sizes can be related to the truncation of the exchange interaction list. Here, both models predicted a reduction of T_C when the range of truncation is less than 3 unit cell sizes. Moreover, the finite model also put in evidence the finite-size effects previously demonstrated by experiment and simulation.

ACKNOWLEDGMENTS

The authors are grateful to Advanced Storage Technology Consortium for financial support and all simulations have been done using the high-performance computing (HPC) facility provided by the University of York.

[1] S. Sun, C. B. Murray, D. Weller, L. Folks, and A. Moser, Science **287**, 1989 (2000).
[2] D. Weller, O. Mosendz, G. Parker, S. Pisana, and T. S. Santos, Phys. Status Solidi A **210**, 1245 (2013).
[3] D. Weller, A. Moser, L. Folks, M. Best, W. Lee, M. Toney, M. Schwickert, J.-U. Thiele, and M. Doerner, IEEE Trans. Magn. **36**, 10 (2000).
[4] A. Q. Wu, Y. Kubota, T. Klemmer, T. Rausch, C. Peng, Y. Peng, D. Karns, X. Zhu, Y. Ding, E. K. Chang *et al.*, IEEE Trans. Magn. **49**, 779 (2013).
[5] T. W. McDaniel, J. Phys.: Condens. Matter **17**, R315 (2005).
[6] R. F. L. Evans, U. Atxitia, and R. W. Chantrell, Phys. Rev. B **91**, 144425 (2015).
[7] M. D. Kuz'min, Phys. Rev. Lett. **94**, 107204 (2005).
[8] C.-B. Rong, D. Li, V. Nandwana, N. Poudyal, Y. Ding, Z. L. Wang, H. Zeng, and J. P. Liu, Adv. Mater. **18**, 2984 (2006).
[9] O. Hovorka, S. Devos, Q. Coopman, W. J. Fan, C. J. Aas, R. F. L. Evans, X. Chen, G. Ju, and R. W. Chantrell, Appl. Phys. Lett. **101**, 052406 (2012).
[10] M. V. Fistul and A. V. Ustinov, Phys. Rev. B **63**, 024508 (2000).
[11] G. Finocchio, F. Büttner, R. Tomasello, M. Carpentieri, and M. Kläui, J. Phys. D: Appl. Phys. **49**, 423001 (2016).
[12] Y. Zhou, E. Iacocca, A. A. Awad, R. K. Dumas, F. Zhang, H. B. Braun, and J. Åkerman, Nat. Commun. **6**, 8193 (2015).
[13] D. A. Allwood, G. Xiong, C. Faulkner, D. Atkinson, D. Petit, and R. Cowburn, Science **309**, 1688 (2005).
[14] N. Papanicolaou and T. Tomaras, Nucl. Phys. B **360**, 425 (1991).
[15] J. P. Attané, M. Tissier, A. Marty, and L. Vila, Phys. Rev. B **82**, 024408 (2010).
[16] L. Nottale, *Scale Relativity and Fractal Space-Time: A New Approach to Unifying Relativity and Quantum Mechanics* (World Scientific, Singapore, 2011).
[17] I. Merches and M. Agop, *Differentiability and Fractality in Dynamics of Physical Systems* (World Scientific, Singapore, 2015).
[18] O. N. Mryasov, U. Nowak, K. Y. Guslienko, and R. W. Chantrell, Europhys. Lett. **69**, 805 (2005).
[19] D. Hinzke, N. Kazantseva, U. Nowak, O. N. Mryasov, P. Asselin, and R. W. Chantrell, Phys. Rev. B **77**, 094407 (2008).
[20] C. Kittel, *Thermal Physics* (Academic Press, New York, 1969), pp. 1–26.
[21] B. Giovannini, M. Peter, and J. R. Schrieffer, Phys. Rev. Lett. **12**, 736 (1964).
[22] S. Blundell, *Magnetism in Condensed Matter* (Oxford University Press, Oxford, UK, 2001).
[23] P. Bruno and C. Chappert, Phys. Rev. Lett. **67**, 1602 (1991).
[24] M. Rezaei, J. Abouie, and F. Nazari, Phys. Rev. B **106**, 064407 (2022).
[25] M. A. Ruderman and C. Kittel, Phys. Rev. **96**, 99 (1954).
[26] A. O. Leon, J. d'Albuquerque e Castro, J. C. Retamal, A. B. Cahaya, and D. Altbir, Phys. Rev. B **100**, 014403 (2019).
[27] H.-R. Chang, J. Zhou, S.-X. Wang, W.-Y. Shan, and D. Xiao, Phys. Rev. B **92**, 241103(R) (2015).
[28] D. Suess, S. Koraltan, F. Slanovc, F. Bruckner, and C. Abert, Phys. Rev. B **107**, 104424 (2023).
[29] C. Auffray and L. Nottale, Prog. Biophys. Mol. Biol. **97**, 79 (2008).
[30] Z. Fu, S. Liu, S. Liu, and Q. Zhao, Phys. Lett. A **290**, 72 (2001).
[31] K. Hosseini, K. Sadri, E. Hinçal, S. Sirisubtawee, and M. Mirzazadeh, Optik **288**, 171176 (2023).
[32] R. F. L. Evans, W. J. Fan, P. Chureemart, T. A. Ostler, M. O. A. Ellis, and R. W. Chantrell, J. Phys.: Condens. Matter **26**, 103202 (2014).
[33] K. Sato, B. Bian, T. Hanada, and Y. Hirotsu, Scr. Mater. **44**, 1389 (2001).
[34] P. Asselin, R. F. L. Evans, J. Barker, R. W. Chantrell, R. Yanes, O. Chubykalo-Fesenko, D. Hinzke, and U. Nowak, Phys. Rev. B **82**, 054415 (2010).
[35] M. Farle, K. Baberschke, U. Stetter, A. Aspelmeier, and F. Gerhardter, Phys. Rev. B **47**, 11571 (1993).
[36] N. T. Binh, S. Ruta, O. Hovorka, R. F. L. Evans, and R. W. Chantrell, Phys. Rev. B **106**, 054421 (2022).
[37] R. F. L. Evans, Q. Coopman, S. Devos, W. J. Fan, O. Hovorka, and R. W. Chantrell, J. Phys. D **47**, 502001 (2014).
[38] S. Okamoto, N. Kikuchi, O. Kitakami, T. Miyazaki, Y. Shimada, and K. Fukamichi, Phys. Rev. B **66**, 024413 (2002).